Contents lists available at ScienceDirect

Physics Letters B

Investigation of the role of ^{10}Li resonances in the halo structure of ^{11}Li through the ^{11}Li(p, d)^{10}Li transfer reaction

A. Sanetullaev [a,b,1], R. Kanungo [a,*], J. Tanaka [c], M. Alcorta [b], C. Andreoiu [d], P. Bender [b], A.A. Chen [e], G. Christian [b], B. Davids [b], J. Fallis [b], J.P. Fortin [a,f], N. Galinski [b], A.T. Gallant [b], P.E. Garrett [g], G. Hackman [b], B. Hadinia [g], S. Ishimoto [h], M. Keefe [a], R. Krücken [b,i], J. Lighthall [b], E. McNeice [e], D. Miller [b], J. Purcell [a], J.S. Randhawa [a], T. Roger [j], A. Rojas [b], H. Savajols [j], A. Shotter [k], I. Tanihata [c,l], I.J. Thompson [m], C. Unsworth [b], P. Voss [d], Z. Wang [b,d]

[a] *Astronomy and Physics Department, Saint Mary's University, Halifax, NS B3H 3C3, Canada*
[b] *TRIUMF, Vancouver, BC V6T2A3, Canada*
[c] *RCNP, Osaka University, Mihogaoka, Ibaraki, Osaka 567 0047, Japan*
[d] *Department of Chemistry, Simon Fraser University, Burnaby, BC V5A 1S6, Canada*
[e] *Department of Physics and Astronomy, McMaster University, Hamilton, ON L8S 4M1, Canada*
[f] *Department of Physics, University of Laval, Quebec City, QB G1V 0A8, Canada*
[g] *Department of Physics, University of Guelph, Guelph, ON N1G 2W1, Canada*
[h] *High Energy Accelerator Research Organization (KEK), Ibaraki 305-0801, Japan*
[i] *Department of Physics and Astronomy, University of British Columbia, Vancouver, BC V6T 1Z1, Canada*
[j] *Grand Accélérateur National d'Ions Lourds, CEA/DSM-CNRS/IN2P3, B.P. 55027, F-14076 Caen Cedex 5, France*
[k] *University of Edinburgh, Edinburgh, United Kingdom*
[l] *School of Physics and Nuclear Energy Engineering and IRCNPC, Beihang University, Beijing 100191, China*
[m] *Lawrence Livermore National Laboratory, L-414, Livermore, CA 94551, USA*

A R T I C L E   I N F O

A B S T R A C T

The first measurement of the one-neutron transfer reaction ^{11}Li(p,d)^{10}Li performed using the IRIS facility at TRIUMF with a 5.7A MeV ^{11}Li beam interacting with a solid H_2 target is reported. The ^{10}Li residue was populated strongly as a resonance peak with energy $E_r = 0.62 \pm 0.04$ MeV having a total width $\Gamma = 0.33 \pm 0.07$ MeV. The angular distribution of this resonance is characterized by neutron occupying the $1p_{1/2}$ orbital. A DWBA analysis yields a spectroscopic factor of 0.67 ± 0.12 for $p_{1/2}$ removal strength from the ground state of ^{11}Li to the region of the peak.

The nuclear halo, discovered three decades back [1,2], continues to be an intriguing object of study posing a great challenge to understand from first principles. Particularly unusual structures are the Borromean neutron halo nuclei, which are weakly bound states of three components, a core nucleus plus two neutrons [1,2]. Here any two sub-components taken together are neutron-unbound. Borromean two-neutron halos have been identified in ^{6}He, ^{11}Li, ^{14}Be, ^{17,19}B [3] and ^{22}C [4]. The challenge to achieve a complete understanding of the Borromean halo relates to the current limited knowledge on the structure and interactions of the pair-wise sub-components. While the sub-components are neutron unbound, some of them can exist as resonances, such as the core-neutron systems, ^{10}Li, ^{13}Be, ^{16,18}B and ^{21}C.

The wavefunction of ^{11}Li can be expressed by a superposition of different resonance states of ^{10}Li plus a neutron that occupies

the relevant matching orbital, in total giving the ^{11}Li ground state a spin of $3/2^-$. In order to understand the dominating ^{10}Li state that constitutes the ground state of ^{11}Li, we report the first measurement of a one-neutron pickup reaction ^{11}Li(p,d)^{10}Li, that transfers neutron from ^{11}Li populating the states in ^{10}Li.

The unbound states of ^{10}Li have been explored through various techniques, but most of these do not relate to the wavefunction of ^{11}Li. ^{10}Li is just beyond the drip-line of the $N = 7$ isotones where it is known that the intruder $2s_{1/2}$ orbital maybe energetically lower than the $1p_{1/2}$ orbital causing a breakdown of the $N = 8$ shell closure. The first observation of a ^{10}Li identified through the ^{9}Be(^{9}Be,^{8}B)^{10}Li reaction [5], found a peak at resonance energy $E_r = 0.80 \pm 0.25$ MeV; $\Gamma = 1.2 \pm 0.3$ MeV (Γ = full width at half maximum). This was later understood not to be the ground state. A subsequent study through the ^{11}B(π^-,^{9}Li+n)p reaction [6] showed a broad structure at $E_r = 0.15 \pm 0.15$ MeV that was assumed to result from a large s-wave amplitude. This assumption is supported by observation of an $l = 0$ resonance at 0.1 ± 0.1 MeV ($\Gamma = 0.4 \pm 0.1$ MeV) in the ^{11}B(π^-,p)^{10}Li reaction [7]. A resonant state unbound to neutron decay by at least 100 keV, and with a possible s-wave or p-wave structure was identified from a study of the ^{11}B(^{7}Li,^{8}B)^{10}Li reaction [8].

The presence of a neutron s-wave in the lowest state of ^{10}Li was further affirmed from several fragmentation experiments. The relative-velocity spectrum of the ^{9}Li-n system from fragmentation of ^{18}O was peaked at zero indicative of the s-wave nature [9,10], with a scattering length, $a_s < -20$ fm [10]. Momentum distributions of one proton and one-neutron removal from ^{11}Be [11] and ^{11}Li [12], respectively were rather narrow which indicates that a neutron in the ^{10}Li ground state has a strong s-wave component. The invariant mass spectrum from a ^{9}Li-n coincidence measurement, following neutron removal from ^{11}Li, when analyzed using a Breit–Wigner distribution shows the lowest resonance at $E_r = 0.21 \pm 0.05$ MeV; $\Gamma = 0.12^{+0.10}_{-0.05}$ MeV [13]. The neutron removal reactions suggest the s-wave virtual state to have a scattering length varying in the range $a_s \sim -22$ to -30 fm [14,15].

Several studies have suggested the first excited state of ^{10}Li to be a $p_{1/2}$ resonance. The ^{9}Li(d,p) reaction [16] exhibits a peak at $E_r \sim 0.38$ MeV interpreted as this resonance. This peak is much lower in energy than that in Ref. [5]. ^{10}Be(^{12}C, ^{12}N)^{10}Li is the only other measurement [17] which showed an even lower energy peak at 0.24 ± 0.04 MeV together with a peak at 0.53 ± 0.06 MeV which are both $l = 1$ resonances. The latter resonance energy seems consistent with the observation from the ^{9}Be(^{9}Be,^{8}B) reaction reporting an $l = 1$ resonance at 0.50 ± 0.06 MeV [18], but not consistent with the 0.8 MeV state in Ref. [5]. The resonances observed at 0.54 ± 0.06 MeV in the ^{11}B(^{7}Li,^{8}B)^{10}Li reaction [8], and at 0.7 ± 0.2 MeV in the ^{11}B(π^-,p) reaction [7], are also in agreement with the above. The two-proton removal from ^{12}B reports three positive parity resonances at 0.1 ± 0.04 MeV, 0.5 ± 0.1 MeV and 1.1 ± 0.1 MeV [19]. The decay spectrum is dominated by the 0.5 ± 0.1 MeV resonance exhibiting a peak but the other two components were required in order to fit the rising and trailing edges of the spectrum. Recently, stopped π^- absorption reactions with ^{14}C target reported peaks for ^{10}Li at $E_r = 0.70 \pm 0.05$ MeV and 0.78 ± 0.15 MeV [20].

While all of the above mentioned reactions can probe the excited resonance spectrum of ^{10}Li, they do not convey information on the role of these resonances in the ground state structure of ^{11}Li. This can be investigated via neutron removal or neutron transfer reactions from ^{11}Li. Several neutron removal reactions exhibited peaks at $E_r = 0.61 \pm 0.10$ MeV [13], 0.68 ± 0.10 MeV [23], 0.510 ± 0.044 MeV [15] and 0.566 ± 0.014 MeV [14]. The resonance energies were obtained from Breit–Wigner fits of the ^{9}Li-n decay energy spectra, with a sum of contributions from resonances
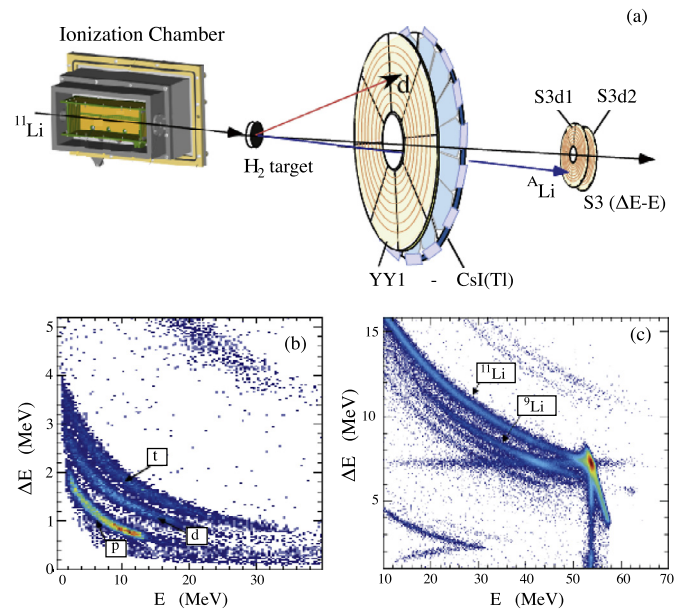

Fig. 1. (a) A schematic layout of the experiment. The particle identification using the (b) YY1-CsI(Tl) array (c) S3 $\Delta E - E$ array.

whose widths depend on the decay energy and angular momentum. This led to an understanding of the $l = 1$ nature of the peak while the lower energy spectrum shows a strong and narrow contribution from the $l = 0$ virtual state. These measurements however do not provide any information on the spectroscopic factor that is necessary to define the ground state of ^{11}Li. A neutron transfer reaction is a decisive way to ascertain both the angular momentum and the spectroscopic strength from the measured angular distribution. The main motivation of the investigation reported in this article is to study the neutron pickup reaction ^{11}Li(p,d)^{10}Li, since no such study has yet been performed.

The first measurement of this one-neutron transfer from ^{11}Li using the IRIS facility [21] at TRIUMF, Canada is reported in this letter. The ^{11}Li beam with an average intensity of 2800 pps, accelerated to an energy of $6A$ MeV using the superconducting LINAC at the ISACII facility, interacted with a solid H_2 target at IRIS. The beam intensity was determined using a low-pressure transmission-type ionization chamber operated with isobutane gas at 19.5 Torr placed before the H_2 target. The energy-loss spectrum of the ionization chamber also revealed that there were no isobaric contaminants in the beam.

The light particles emitted after reactions such as p, d and t were detected using annular arrays of segmented silicon strip detectors (YY1) backed by a CsI(Tl) array. This array covered laboratory angles of $\theta_{lab} = 32°$ to $58°$. The silicon detectors, labeled as YY1 detector, in Fig. 1 are 100 µm thick and largely serve the role of an energy-loss (ΔE) detector. The remaining energy (E) of the light particles after passing through the YY1 detector is measured by the CsI(Tl) array. The particle identification using this $\Delta E - E$ telescope array is shown in Fig. 1b. The scattered deuterons from the (p,d) reaction are seen to be clearly separated from the protons and tritons. In order to deduce the energy of the particles, the detectors were calibrated using the ^{11}Li-p elastic scattering data. The heavy reaction residues pass through the hole in the YY1 annular array, and are detected using a $\Delta E - E$ (60 µm–500 µm thick) double-sided segmented silicon strip detector array, S3, placed further downstream of the target. This telescope covered laboratory angles of $\theta_{lab} = 1.8°$ to $5.7°$. The $\Delta E - E$ spectrum from the S3 arrays allows a clear identification of ^{9}Li (Fig. 1c).

The solid H_2 target was formed by spraying H_2 gas onto a 5.4 μm thick cooled Ag foil. The foil adheres to a copper target cell frame cooled to 4 K. The target thickness was measured using the Ag(^{11}Li,^{11}Li)Ag elastic scattering peak energy of ^{11}Li detected in the S3 silicon array. This was done simultaneously while measuring the (p,d) reaction. The difference in energy of this elastic peak without and with H_2 provides a measure of the solid H_2 thickness from the energy loss within it. It was crucial to have a continuous thickness determination because the target was found to gradually evaporate after several hours. A continuous thickness measurement therefore allowed us unambiguous determination of cross section using the thickness measured at each instant together with the respective number of reaction events. When the thickness dropped below a certain level the target was re-furbished by adding H_2. The average thickness was ~ 60 μm varying from ~ 30 μm to ~ 130 μm with time. In order to restrict the radiative heating of the H_2 target, the target cell is surrounded by a copper heat shield which is cooled to ~ 30 K. The opening of the heat shield for the scattered particles led to an angle dependent geometric efficiency for the Yd1-CsI(Tl) detector array since the shield masks parts of this array. This geometric efficiency was determined by a Monte Carlo simulation. The background reactions from the Ag foil emitting deuterons were negligibly small as found from measurement without the H_2 layer. The beam energy at mid-target was $5.7A$ MeV.

Fig. 2a shows the measured energy-angle scatter plot of deuterons by the YY1-CsI(Tl) telescope. For energies below 4.5 MeV, the deuterons stop in the silicon layer and therefore cannot be identified by the procedure mentioned above. Those events plotted below 4.5 MeV include all particles stopped in the YY1 detector in coincidence with ^{9}Li in the S3 telescope (Fig. 2a). In order to minimize the non-resonant background the azimuthal angle between the deuterons and the ^{9}Li was restricted to $180° \pm 60°$. The region outside this selection does not exhibit any resonance peak.

The resonance energy spectrum (Fig. 2b) of ^{10}Li is constructed in the missing mass technique using the measured energy and scattering angle of the deuterons. A very prominent resonance peak is seen at $E_r = 0.62 \pm 0.04$ MeV and full width $\Gamma = 0.33 \pm 0.07$ MeV is obtained from fitting the spectrum with a Voigt function with an energy dependent Breit–Wigner function width [22]. The average (Gaussian) excitation energy resolution over the range of angles used in this fit is $\sigma \sim 0.31$ MeV based on simulation that reproduces elastic scattering peak width. The resonance peak width extracted is consistent throughout the angular range. The resonance energy is consistent with that reported in Refs. [7,8, 14,15,17,19,23]. The intrinsic width of the peak is in good agreement with observations from multinucleon transfer reactions [8, 17,18] and consistent within large uncertainties with neutron removal reactions [15,14]. The widths reported in Refs. [13,23] are much larger and that in Ref. [7] is much smaller.

The spectrum does not exhibit any other resonance peak(s) such as at $E_r = 0.24$ MeV [17], 0.35 MeV [16] although they would be within the detector acceptance. A higher energy resonance such as $E_r \sim= 1.49$ MeV discussed in [15] is also within the detector acceptance but its absence suggests that it could only be a small component in the ground state of ^{11}Li. The remaining part of the spectrum is estimated with non-resonant background from the three-body phase space of ^{11}Li+p $\rightarrow$ d+^{9}Li+n considering an isotropic emission of the products in the center-of-mass (cm) frame. The simulated shape of this non-resonant contribution folded with the (Gaussian) experimental resolution is shown by the dotted (red) curve in Fig. 2b. This simulated contribution describes fairly well the spectrum with energy higher than the peak region. In addition, there can be background from mixing of other particles for events stopping in the YY1 detector which
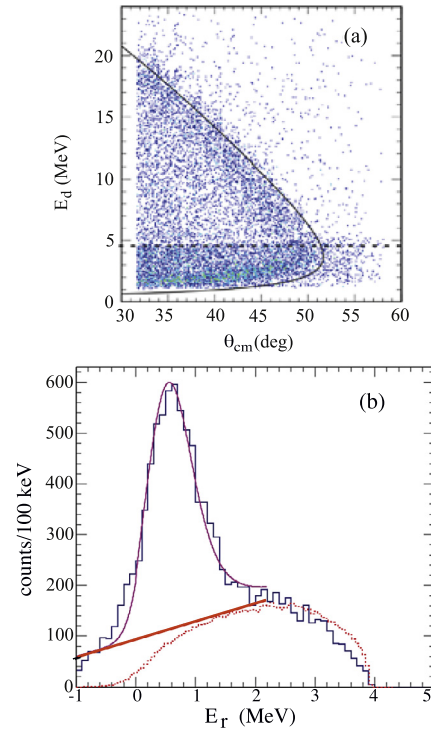

Fig. 2. (a) The correlation of energy of deuterons as a function of laboratory scattering angle. The black curve shows the calculated kinematic locus for ^{10}Li at the ^{9}Li+n threshold (i.e. for $E_r = 0$ MeV). The region below the dashed horizontal line are events that stop in the YY1 detector. (b) The resonance energy spectrum reconstructed from energy and scattering angle measured for the deuterons. The dotted curve shows the calculated ^{9}Li+n+d three-body non-resonant phasespace. The solid (red) line shows the linear background shape considered in the cross section evaluation. The pink curve is the fit to the peak using Breit–Wigner resonance folded with experimental resolution and the linear background. (For interpretation of the references to color in this figure legend, the reader is referred to the web version of this article.)

were not identified as deuterons. Such background events and effects of the experimental resolution contribute to the spectrum extending below $E_r = 0$ MeV. In order to estimate the uncertainty due to the assumed background profile we have also used a second method where the spectrum was fitted by a Breit–Wigner peak folded with the resolution plus a linear background shape (solid red line, Fig. 2b) around the peak region. The uncertainty in background determination from these different methods is 20% and is included in the total uncertainty of the angular distribution data. The background counts under the resonance peak are subtracted in order to get the number of scattered deuterons for the ^{11}Li(p,d)^{10}Li* reaction. The cross section data presented below is from linear background subtraction including effects of the three-body phase space background as 20% uncertainty.

The ^{11}Li(p,p)^{11}Li elastic scattering channel was identified from a coincident detection of protons and ^{11}Li. The excitation energy resolution measured from the ^{11}Li$_{gs}$ peak is 0.56 MeV (FWHM). The elastic scattering angular distribution is shown in Fig. 3. The curve shows the optical model calculation using the code FRESCO [24] with a phenomenological Woods–Saxon potential for the real and imaginary potentials. The surface imaginary potential is a radial derivative of the Woods–Saxon form, and the spin–orbit potential is (1/r) times the radial derivative of the Woods–Saxon function. The potential parameters (Table 1) were determined from a best fit to the elastic scattering angular distribution. The data include statistical and systematic uncertainties. The contributions to the systematic uncertainty are 5% from target thickness, 5% from solid angle efficiency estimation. For the ^{11}Li(p,d) for resonance

Table 1
Optical potential parameters for ^{11}Li+p from a fit of elastic scattering.

V_0 (MeV)	r_0 (fm)	a_0 (fm)	W_V (MeV)	r_I (fm)	a_I (fm)	W_D (MeV)	r_D (fm)	a_D (fm)	V_{so} (MeV)	r_{so} (fm)	a_{so} (fm)
95.93	1.00	1.10	15.00	0.65	0.50	11.90	0.67	1.1	10.70	0.80	0.75

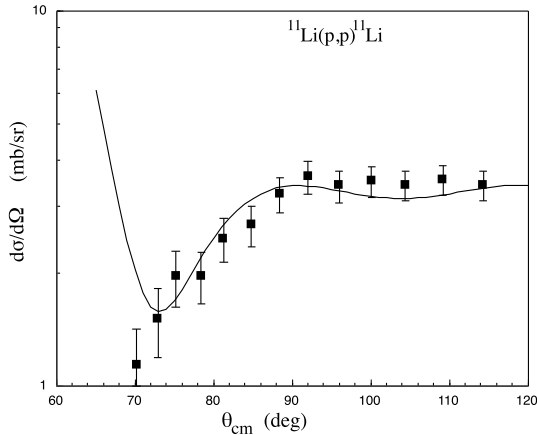**Fig. 3.** The elastic scattering angular distribution data for ^{11}Li(p,p)^{11}Li$_{gs}$. The curve shows optical model calculations with the best fit optical potential parameters.

Fig. 4. The angular distribution data for ^{11}Li(p, d)^{10}Li$_{E_r=0.62\,\text{MeV}}$. The curves show the DWBA calculations. The solid (red) curve/dashed (blue) curve/dotted (black) curve represents one neutron transfer from the $1p_{1/2}/1d_{5/2}/2s_{1/2}$ orbital. The inset shows the detection efficiency.

cross section an additional 20% uncertainty from the background estimation is included.

Fig. 4 shows the angular distribution for the ^{11}Li(p,d)^{10}Li reaction. The detection efficiency shown in the inset of Fig. 4 is based on simulation with the ^{10}Li resonance decaying isotropically in its cm frame into ^{9}Li and neutron. It includes the geometric effect of the heat shield of the target as well as the coincidence efficiency of d and ^{9}Li detection for the forward θ_{cm} angles. The curves in Fig. 4 are DWBA calculations using FRESCO [24]. The exit channel optical potential was considered to be the same as that extracted from the ^{11}Li(d,d) elastic scattering [25]. The single particle form factors have a neutron bound to the proton in a Woods–Saxon potential. The potential is chosen to reproduce the binding energy, root mean square radius, and D_0 of the deuteron. The parameters for the potential are $V_0 = 165.54$ MeV, $r_0 = 0.4$ fm and $a_0 = 0.6$ fm. These are the quantities that affect the transfer cross sections. A Woods Saxon form factor has been used in DWBA calculations in Refs. [26,27]. A comparison of this form factor with a Reid Soft core potential form factor yields $\sim 5\%$ change in spectroscopic factor for the ^{11}Li(p,d)^{10}Li reaction. ^{11}Li is described as a bound state of a ^{10}Li state + a neutron with a Woods–Saxon binding potential where the effective separation energy is $= 0.98$ MeV. The potential has a real and spin–orbit part with same geometry, $r_0 = 1.15$ fm and $a_0 = 0.6$ fm. The depth of the spin–orbit part is $V_{so} = 6$ MeV while the depth of the real part is $V_0 = 49.6$ MeV for a $1p_{1/2}$ neutron.

In the DWBA calculations, we consider three different possibilities of neutron configuration of ^{11}Li for the resonance observed. The solid (red) curve (Fig. 4) shows neutron transfer with angular momentum $l = 1$. The distribution has same shape for transfer from the $1p_{1/2}$ or $1p_{3/2}$ orbital. We consider this neutron transfer to be dominated by transfer from the $1p_{1/2}$ for the discussion below. This consideration is supported by predictions from the Tensor Optimized Shell Model framework that suggests only 2.5% component of $(p_{3/2})^2$ neutrons in ^{11}Li [28]. Neutron transfers from the $2s_{1/2}$ orbital and $1d_{5/2}$ orbital in ^{11}Li are shown by the dotted (black) and dashed (blue) curves, respectively (Fig. 4). The data clearly demonstrate that the resonance peak observed is associated with neutron transfer from the $1p_{1/2}$ orbital. The χ^2_{min} value for
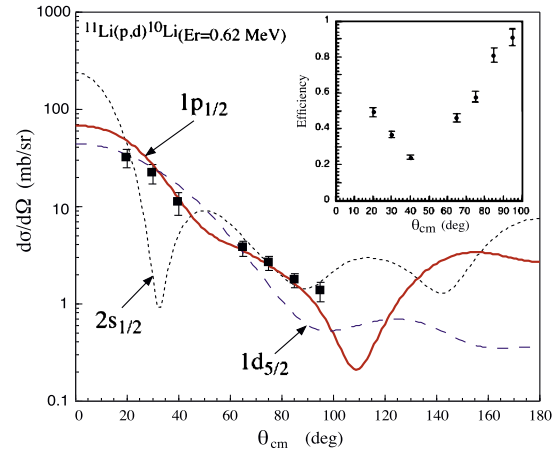
the p-orbital is ~ 0.8 while those for the d- and s-orbital are ~ 4.5 and ~ 6.7, respectively for the best fit normalization to the data. The magnitude of the measured cross section compared to the DWBA calculation provides the spectroscopic factor (S) of this configuration to be 0.67 ± 0.12 with $(d\sigma/d\Omega)_{ex} = S \times (d\sigma/d\Omega)_{DWBA}$. Here, the spectroscopic factor value refers to that of two neutrons. Assuming that the resonance peak observed includes the complete $(1p_{1/2})^2$ strength and hence an overlap of the 1^+ and 2^+ states of ^{10}Li, the probability fraction of the $(1p_{1/2})^2$ component in the wavefunction of ^{11}Li is $S/2 = 0.33 \pm 0.12$, where sum of all components is unity. This is consistent with the predictions in Ref. [28]. Alternatively, if the resonance peak observed is only one of 1^+ or 2^+ states of ^{10}Li with half the p-wave strength, then the total probability fraction of the $1p_{1/2}$ component is $2 \times S/2 = 0.67 \pm 0.12$. We consider the former case to be the more likely situation because the fragmentation reactions also report one resonance peak for the $l = 1$ component [14,15]. In addition, an equally strong second resonance well separated from the present peak and within this excitation energy range should have been observed in this experiment.

If all the remaining component was only $(2s_{1/2})^2$, then this probability fraction would be $\sim 0.67 \pm 0.12$. Recently, 11(2)% of d-wave probability has been found in the ground state of ^{11}Li [29]. Therefore, considering the d-wave, the s-wave probability fraction could be reduced to $\sim 0.56 \pm 0.12$. Fragmentation studies had pointed to an s-wave probability fraction of 0.4 ± 0.1 [30]. The angular distribution of (p,t) two-neutron transfer reaction from ^{11}Li was best explained by wavefunction models with s-wave probability fraction in the range of 0.31–0.45 [31]. The small $(1p_{1/2})^2$ probability observed through the ^{10}Li resonance and hence large $(2s_{1/2})^2$ deduced in the present work agrees with these previous measurements. This value of the s-wave probability fraction deduced here is however higher than that from recent analysis [32] of the reaction cross section reporting an s-wave probability fraction of $0.33^{+0.03}_{-0.05}$. Such a small $(2s_{1/2})^2$ fraction would be consistent only with the assumption that the resonance seen in this work exhibits only half of the $(1p_{1/2})^2$ strength. Calculation in a

three-body model [33] finds that the B(E1) value from Coulomb dissociation is explained by a rather small s-wave probability of 25% while the charge radius was explained using a higher value of 50%. The latter seems to be consistent with the observation in this work. Theoretical developments including multi-step reaction mechanisms would be useful to investigate in future.

In summary, the first measurement of the one-neutron transfer reaction ^{11}Li(p,d)^{10}Li at $E/A = 5.7$ MeV is reported. The excitation spectrum of the ^{10}Li residue is dominated by a strong population of a resonance peak at $E_r = 0.62 \pm 0.04$ MeV with a width $\Gamma = 0.33 \pm 0.07$ MeV. The angular distribution of this resonance analyzed in a one-step DWBA framework confirms it having an $l = 1$ character i.e. with the neutron occupying the $1p_{1/2}$ orbital. The measured cross section yields a spectroscopic factor $= 0.67 \pm 0.12$ for the $(1p_{1/2})^2$ component. This defines relatively small $(p_{1/2})^2$ fraction in ^{11}Li$_{gs}$ associated with this ^{10}Li resonance peak considered to contain the complete $(p_{1/2})^2$ strength. Assuming the remaining probability fraction to be s- and d-waves, a large $(2s_{1/2})^2$ probability fraction $\geq 44\%$ is deduced for the ground state of ^{11}Li. The present observation will serve as guidance for theoretical models calculating more accurate wavefunctions for ^{11}Li.

References

[1] I. Tanihata, et al., Phys. Rev. Lett. 55 (1985) 2676.
[2] P.G. Hansen, B. Jonson, Europhys. Lett. 4 (1987) 409.
[3] I. Tanihata, H. Savajols, R. Kanungo, Prog. Part. Nucl. Phys. 68 (2013) 215.
[4] K. Tanaka, et al., Phys. Rev. Lett. 104 (2010) 062701.
[5] K.H. Wilcox, et al., Phys. Lett. B 59 (1975) 142.
[6] A.I. Amelin, et al., Yad. Fiz. 52 (1990) 1231.
[7] M.G. Gornov, et al., Bull. Russ. Acad. Sci., Phys. 62 (1998) 1781.
[8] B.M. Young, et al., Phys. Rev. C 49 (1994) 279.
[9] R.A. Kryger, et al., Phys. Rev. C 47 (1993) R2439.
[10] M. Thoennessen, et al., Phys. Rev. C 59 (1999) 111.
[11] M. Chartier, et al., Phys. Lett. B 510 (2001) 24.
[12] M. Zinser, et al., Phys. Rev. Lett. 75 (1995) 1719.
[13] M. Zinser, et al., Nucl. Phys. A 619 (1997) 151.
[14] Yu. Aksyutina, et al., Phys. Lett. B 666 (2008) 430.
[15] H. Simon, et al., Nucl. Phys. A 791 (2007) 267.
[16] H.B. Jeppessen, et al., Phys. Lett. B 642 (2006) 449.
[17] H.G. Bohlen, et al., Nucl. Phys. A 616 (1997) 254.
[18] J. Caggiano, et al., Phys. Rev. C 60 (1999) 064322.
[19] J.K. Smith, et al., Nucl. Phys. A 940 (2015) 235.
[20] B.A. Chenyskev, et al., Eur. Phys. J. A 49 (2013) 68.
[21] H. Simon, et al., Nucl. Phys. A 734 (2004) 323.
[22] R. Kanungo, Hyperfine Interact. 225 (2014) 235.
[23] T. Al Kalanee, et al., Phys. Rev. C 88 (2013) 034301.
[24] I.J. Thompson, Comput. Phys. Rep. 7 (1988) 167.
[25] R. Kanungo, et al., Phys. Rev. Lett. 114 (2015) 192502.
[26] G. Potel, F.M. Nunes, I.J. Thompson, Phys. Rev. C 92 (2015) 034611.
[27] R. Kanungo, et al., Phys. Lett. B 682 (2010) 391.
[28] T. Myo, et al., Prog. Theor. Phys. 119 (2008) 561.
[29] Yu. Aksyutina, et al., Phys. Lett. B 718 (2013) 1309.
[30] H. Simon, et al., Phys. Rev. Lett. 83 (1999) 496.
[31] I. Tanihata, et al., Phys. Rev. Lett. 110 (2008) 192502.
[32] H.T. Fortune, Phys. Rev. C 91 (2015) 017303.
[33] H. Esbensen, et al., Phys. Rev. C 76 (2007) 024302.